Proceedings of the 2017 IEEE
International Conference on Robotics and Biomimetics
December 5-8, 2017, Macau SAR, China

Pareto-Front Analysis of a Monotonic PI Control Law for Slip Suppression in a Robotic Manipulator

Anna Prach[1], John-John Cabibihan[2], Nitish V. Thakor[1], and Dennis S. Bernstein[3]

Abstract— **This paper presents a novel slip-suppression controller for a two-fingered robotic manipulator, where the goal is to minimize the slip distance without using excessive force. To do this, we consider monotonic PI (MPI) control, which is a nonlinear extension of linear proportional-integral (PI) control. The advantage of MPI control is the fact that the normal force of the gripper is prohibited from decreasing during the transition from predominantly proportional control to predominantly integral control as occurs in the case of linear PI control. The performance of the MPI control is compared to linear PI control for a range of controller parameters, and the tradeoff between the maximum normal force and the total slip distance is efficiently captured by Pareto-front analysis. The robustness of MPI is assessed by considering uncertainty in the body mass and friction parameters, as well as the effect of measurement noise and actuator dynamics.**

I. INTRODUCTION

One of the main challenges in controlling robotic end effectors is to determine the grip force necessary to avoid slippage of an object without applying excessive grip force; this requirement is critical for fragile and delicate objects. Slip suppression is thus particularly important when manipulating objects with uncertain or varying mass and surface roughness.

The first stage of slip suppression is to detect the onset of slip. This requires a sensor that can detect motion of the object relative to the end effector. Optical sensors are used to detect slip in [1], [2]; slip detection based on the tangential (shear) force derivative is presented in [3]–[5]; slip detection using strain gauges is reported in [6]; and center of pressure tactile sensors are used to detect slip in [7].

Various techniques for slip suppression are presented in literature. The control algorithm in [1], which is based on tactile and optical sensors mounted on the fingertips, regulates grip pressure and prevents object slippage during manipulation. In [3], slip suppression is addressed using nonlinear model predictive control. A proportional-derivative shear-force feedback control and adaptive slip prevention algorithm are explored in [4], [6]. In yet another approach, the controller in [2] adjusts the grip force based on the slip distance. Normal force is typically regulated by feedback from force sensors or tactile sensors, which are extensively used in prosthetics and robotics [8], [9].

According to human physiology, humans adjust their grip force in response to sensed friction [10]–[12]. Results in [13] show that the friction force between the skin and grasped object is essential for determining a force that is sufficient for a secure grip. Various friction models describe the friction force as a function of the normal force, slip velocity, and friction parameters [14]–[18]. The relation between the normal (grip) force and the tangential (friction) is essential for modeling the dynamics of a slipping body, simulate slip events, design and validate the control laws [19]. In [20], [21], slip models based on Coulomb friction are used for slip-suppression control design. The LuGre friction model is used for online slip prediction and compensation in [22].

From the control point of view, the problem of slip suppression can be viewed as a problem of finite-arc-length stabilization, which implies that the closed-loop trajectories converge to an equilibrium state in a finite distance [23]. A sufficient condition for finite slip distance (FSD) is finite-time convergence (FTC) [24]. The converse it not true, however, since FSD may be achievable with exponential convergence of the velocity to zero.

In this work, we develop and analyze a slip-suppression controller for a two-fingered robotic end effector. The end effector holds a rigid body of arbitrary shape, which moves (slips) in a vertical plane. A simulation model of the end effector with Coulomb friction is used to simulate slip events and assess performance of the slip-suppression controller.

Although the normal force is limited in practice by properties of the hardware, the goal is to minimize the slip distance without applying excessive force and thus obtain an efficient tradeoff between normal force and slip distance. We consider monotonic PI (MPI) control, which is a nonlinear extension of linear PI control. The advantage of MPI control is the fact that the normal force of the gripper is restricted from decreasing during the transition from predominantly proportional control to predominantly integral control, as occurs in the case of linear PI control. The performance of MPI control is compared to linear PI control for a range of controller parameters, and the tradeoff between the maximum normal force and the total slip distance is efficiently captured by Pareto-front analysis. The robustness of MPI is assessed by considering uncertainty in the body mass and friction parameters, as well as the effect of measurement noise and actuator dynamics.

This paper is organized as follows. Section II describes the dynamics of the end effector-body system and friction

[1]Anna Prach and Nitish V. Thakor are with Singapore Institute for Neurotechnology, National University of Singapore, 117456 Singapore. annaprach@me.com, sinapsedirector@gmail.com

[2]John-John Cabibihan is with the Mechanical and Industrial Engineering Department, Qatar University, 2713, Doha, State of Qatar john.cabibihan@qu.edu.qa

[3]Dennis S. Bernstein is with the Aerospace Engineering Department, University of Michigan, Ann Arbor, MI 48109, USA dsbaero@umich.edu

978-1-5386-3741-8/17/$31.00 © 2017 IEEE

model. Section III covers control architecture, convergence analysis, and numerical investigation of the closed-loop response. Robustness analysis including robustness to constant disturbances, uncertain friction, actuator dynamics, and sensor noise is given in Section IV. Section V summarizes discussion on the results, conclusions and future work.

II. End Effector-Body Dynamics and Friction Model

Consider a body with mass m held by a two-fingered robotic end effector, the schematic view of which is shown in Fig. 1, where $q(t)$ is the position of the body relative to the zero reference on the end effector, $f_{\rm n}(t) \geq 0$ is the normal force applied by the end effector in response to the normal force requested by the controller, $f_{\rm d}(t)$ is the disturbance force applied to the body, and $f_{\rm f}(t)$ is the friction force applied to the body due to $f_{\rm n}(t)$. Gravity with acceleration g acts along the x-axis. If $\dot{q} = 0$ then the body is fixed relative to the end effector fingers, and thus no slipping occurs. If $\dot{q} \neq 0$, then the body is slipping relative to the end effector. Since the force on the body due to gravity is mg, the

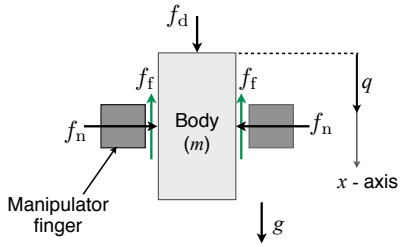

Fig. 1. Two-fingered robotic manipulator and body.

effect of a constant disturbance is to either increase the effect of gravity (if the disturbance force is positive) or decrease the effect of gravity (if the disturbance force is negative). Hence, robustness to mass uncertainty is equivalent to robust rejection of uncertain constant disturbances. Therefore, there is no need to consider the case of constant disturbances.

The equation of motion of the body is given by

$$m\ddot{q}(t) = mg + f_{\rm d}(t) - f_{\rm f}(t), \tag{1}$$

where friction force $f_{\rm f}(t)$ is defined by the friction model. In terms of the velocity $v(t) \triangleq \dot{q}(t)$ of the body, (1) becomes

$$m\dot{v}(t) = mg + f_{\rm d}(t) - f_{\rm f}(t). \tag{2}$$

The disturbance force may be positive or negative, hence, the body may be moving upwards. Note that $f_{\rm n}$ is physically constrained to be nonnegative. However, throughout the paper, we assume that $v(t)$ is nonnegative, and thus this constraint is satisfied for all control laws. Thus, the primary objective is to prevent the body from slipping downwards.

The *slip distance* $\delta(t)$ is defined as

$$\delta(t) \triangleq q(t) - q(0) = \int_0^t v(\tau)\,{\rm d}\tau - q(0) \geq 0, \tag{3}$$

and thus the *asymptotic slip distance* is given by

$$\delta_\infty \triangleq \lim_{t\to\infty} \delta(t). \tag{4}$$

Consider the Coulomb friction model given by [15]

$$f_{\rm f} = \begin{cases} f_{\rm C}{\rm sgn}(v), & v \neq 0, \\ \min(|f_{\rm d}|, f_{\rm st}){\rm sgn}(f_{\rm d}), & v = 0, \end{cases} \tag{5}$$

where the Coulomb friction force $f_{\rm C}$ and the static friction force $f_{\rm st}$ are given by

$$f_{\rm C} = \mu f_{\rm n}, \tag{6}$$

$$f_{\rm st} = \mu_{\rm st} f_{\rm n}, \tag{7}$$

where $\mu > 0$ is the sliding friction coefficient and $\mu_{\rm st} > 0$ is the static friction coefficient. Stick condition occurs when $v = 0$. A particular nonlinear effect captured by this friction model is stick-slip, which is a consequence of lower friction force during slip. During stick, the direction of the friction force is defined by the direction of the disturbance force $f_{\rm d}$. During slip, the friction force $f_{\rm f}$ is equal to $f_{\rm C}$ or $-f_{\rm C}$, depending on the sliding direction.

III. Slip-Suppression Control

The slip-suppression controller regulates the normal force $f_{\rm n}$ in order to bring the slip velocity v to zero with the smallest possible slip distance without excessive normal force. The block diagram of the control system is shown in Fig 2, where the gripper-body dynamics are given by (2), friction model is given by (5) and (6), and w represents sensor noise, which is assumed as the Gaussian white noise. The normal force requested by the controller and applied by the actuator mechanism is $f_{\rm n}$. The reference command is $v_{\rm ref} = 0$, and thus the slip-velocity error e is defined by $e(t) \triangleq v_{\rm ref}(t) - v(t) = -v(t)$. The controller is represented by either linear or nonlinear PI control law.

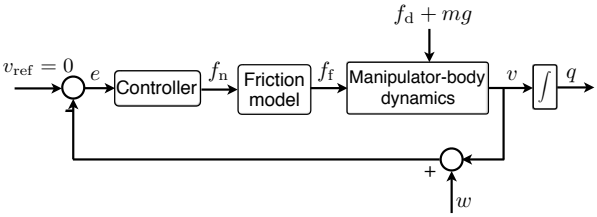

Fig. 2. Feedback control architecture.

Consider the PI controller

$$\dot{h} = v, \tag{8}$$

$$f_{\rm n} = K_{\rm I} h + K_{\rm P} v, \tag{9}$$

where $K_{\rm P} \geq 0$ and $K_{\rm I} \geq 0$ are the proportional and integral gains, respectively.

A. Convergence Analysis

For convergence analysis, note that the proportional term $K_{\rm P}v$ in (9) is essential for stabilization assuming no constant disturbance, while the integral term $K_{\rm I}h$ rejects the effect of gravity and constant disturbances.

First, we consider stabilization without constant disturbance. The closed-loop dynamics with a linear proportional control are given by

$$m\dot{v} = -f_{\rm f} = -\mu f_{\rm n} = -\mu K_{\rm P} v. \tag{10}$$

Solving (10) yields

$$v(t) = v_0 e^{-\frac{\mu K_\mathrm{P}}{m} t}, \tag{11}$$

which shows that the slip velocity decays exponentially for $K_\mathrm{P} > 0$.

For PI control considering a constant disturbance (gravity), the closed-loop dynamics are given by

$$\begin{aligned} m\dot{v}(t) &= -\mu f_\mathrm{n}(t) + mg \\ &= -\mu(K_\mathrm{P} v(t) + K_\mathrm{I} \int_0^t v(\tau)\mathrm{d}\tau) + mg. \end{aligned} \tag{12}$$

Differentiating (12) yields

$$\ddot{v} + \frac{\mu K_\mathrm{P}}{m}\dot{v} + \frac{\mu K_\mathrm{I}}{m} v = 0. \tag{13}$$

Since (13) is a linear second-order ODE with constant positive coefficients, the slip velocity decays exponentially with or without oscillation depending on whether (13) is underdamped or overdamped, respectively.

B. Numerical Investigation

For numerical study, let $m = 1$ kg, $\mu_\mathrm{st} = 1$, and $\mu = 0.7$.

1) Effect of K_P and K_I on the Closed-Loop Performance: To study how feedback gains K_P and K_I effect the closed-loop performance, we consider two cases, namely fixed K_I and varying K_P, and vice versa. First, let $K_\mathrm{I} = 30$ N/m and $K_\mathrm{P} \in \{10, 20, 30\}$ N-s/m. The corresponding closed-loop response with $v_0 = 1$ m/s is shown in Fig. 3. Next, let $K_\mathrm{P} = 10$ N-s/m and $K_\mathrm{I} \in \{10, 20, 30\}$ N/m. The corresponding closed-loop response with $v_0 = 1$ m/s is shown in Fig. 4.

Although these cases demonstrate how K_P and K_I affect the closed-loop performance, they do not provide a methodology for choosing PI gains that provide an efficient tradeoff between MNF and TSD. The next section addresses this problem in terms Pareto optimality.

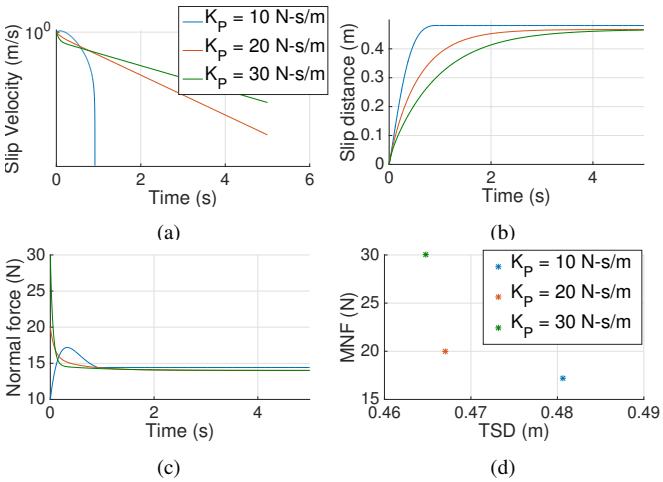

Fig. 3. PI control with $v_0 = 1$ m/s, $K_\mathrm{I} = 30$ N/m, and $K_\mathrm{P} \in \{10, 20, 30\}$ N-s/m. a) shows the slip velocity; FTC is achieved with $K_\mathrm{P} = 10$ N-s/m. b) shows the slip distance; FSD is achieved with all values of gains. c) shows the normal force, and d) shows the corresponding MNF and TSD values. Note that larger K_P yields larger MNF and smaller TSD.

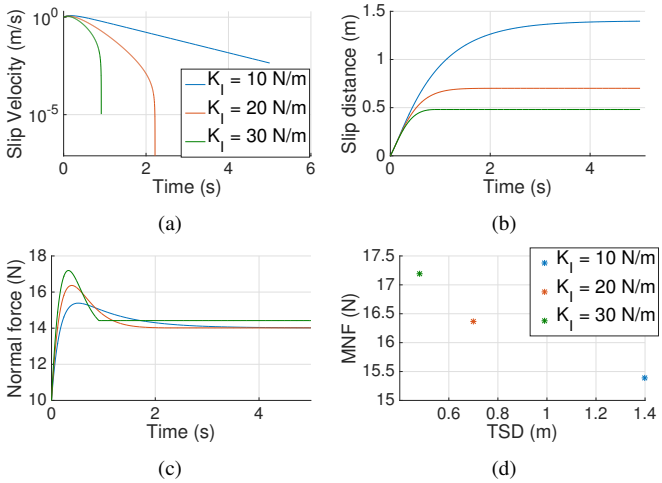

Fig. 4. PI control with $v_0 = 1$ m/s, $K_\mathrm{P} = 10$ N-s/m, and $K_\mathrm{I} \in \{10, 20, 30\}$ N/m. a) and b) show slip velocity and slip distance, respectively; FTC is achieved with $K_\mathrm{I} \in \{20, 30\}$ N/m, while FSD is achieved all considered gains. c) shows normal force, and d) show corresponding MNF and TSD values. Larger K_I yields larger MNF and smaller TSD.

2) Pareto-Optimal Front for PI Control: Motivated by multi-objective optimization, we apply Pareto efficiency analysis to construct the Pareto-optimal front that is the optimal tradeoff curve between MNF and TSD obtained for a given range of feedback gains. Pareto-optimal curve also allows to determine the corresponding Pareto-optimal gains from the given range.

We consider stabilization and gravity compensation with $v_0 = 1$ m/s. Let K_P range from 10 N-s/m to 100 N-s/m, and K_I range from 10 N/m to 500 N/m. For each pair $K_\mathrm{P}, K_\mathrm{I}$, the MNF and TSD values are computed for a fixed simulation time equal to 10 sec, and result to suboptimal MNF/TSD values as shown in Fig. 5 a). Next, the suboptimal MNF/TSD values are removed yielding the Pareto-optimal front, as shown in Fig. 5 a), where each point on the Pareto-optimal front represents optimal tradeoff between MNF and TSD. This procedure results to a set of *Pareto-optimal gains* K_P and K_I that correspond to the MNF-TSD points on the Pareto-optimal front, as shown in Fig. 5 b). Figure 6 a) and b) show the Pareto-optimal gains versus TSD and MNF, respectively. Note that TSD approaches zero as MNF goes to infinity. Hence, it is possible to attain arbitrarily small slip distance using high levels of normal force.

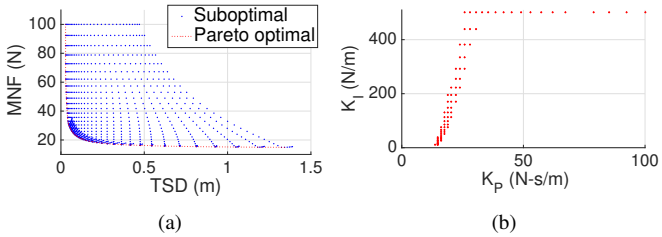

Fig. 5. PI control with $v_0 = 1$ m/s. a) shows the resulting tradeoff between MNF and TSD, and highlight the Pareto-optimal front. b) shows the corresponding values of the Pareto-optimal gains.

3) Monotonic PI Control: For PI control, Fig. 3 and 4 show that f_n decreases after reaching peak value. This decrease may, however, lead to an increase in the slip

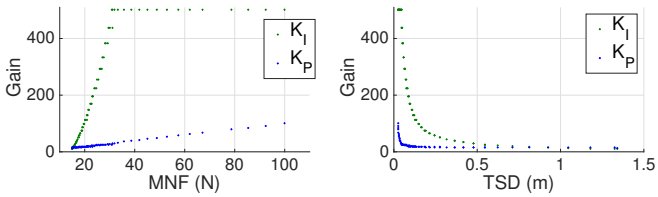

(a) (b)

Fig. 6. PI control with $v_0 = 1$ m/s. a) shows the Pareto-optimal gains K_P and K_I versus MNF, while b) shows the same gains versus TSD.

distance as compared to maintaining the normal force. Since the tradeoff between MNF and TSD only considers the peak value of the normal force, we propose a modified PI control where f_n can only increase but not decrease. In the modified control law, at every time step, the current value of f_n is compared to its value at the previous time step, selecting the largest of these two values to be used at the next step. The resulting f_n is thus monotonically nondecreasing as a function of time, hence the controller is a *monotonic PI* control law. Although the modified controller does not change MNF, it may reduce TSD in cases where f_n given by the PI control decreases. Note that, whereas PI control is linear, MPI is nonlinear. The closed-loop response for MPI control with $v_0 = 1$ m/s, $K_\mathrm{P} = 10$ N-s/m, and $K_\mathrm{I} \in \{10, 20, 30\}$ N/m is given in Fig. 7, which show that monotonic PI yields faster velocity convergence and smaller TSD as compared to conventional PI control.

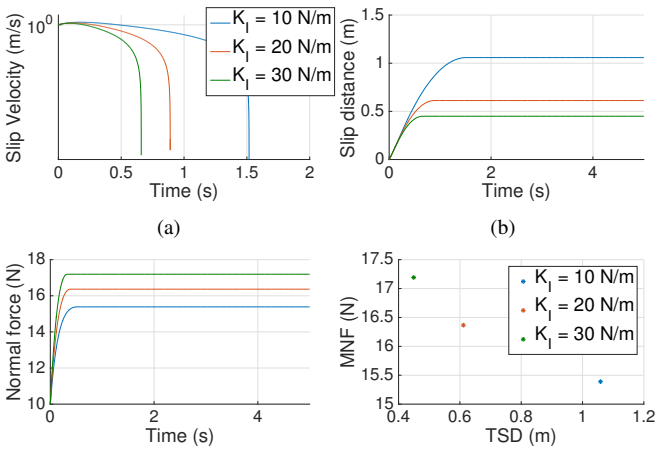

(a) (b) (c) (d)

Fig. 7. MPI control with $v_0 = 1$ m/s, $K_\mathrm{P} = 10$ N-s/m, $K_\mathrm{I} \in \{10, 20, 30\}$ N/m. a) and b) show slip velocity and slip distance, respectively; note that FTC and FSD is achieved with all three values of K_I. c) shows that f_n does not decrease after MNF is reached, while d) shows the corresponding MNF and TSD values.

4) Pareto Analysis of MPI Control: For Pareto analysis, we consider stabilization and gravity compensation with $v_0 = 1$ m/s. Let K_P range from 10 N-s/m to 100 N-s/m, and K_I range from 10 N/m to 500 N/m. Each pair $K_\mathrm{P}, K_\mathrm{I}$ yields suboptimal MNF/TSD values, shown in Fig. 8 a). Removing suboptimal MNF/TSD values, yields the Pareto-optimal front, with the corresponding Pareto-optimal gains K_P and K_I, as shown in Fig. 8. Figure 9 a) and b) show the Pareto-optimal gains versus TSD and MNF, respectively. Same as for PI control, TSD approaches zero as MNF goes to infinity.

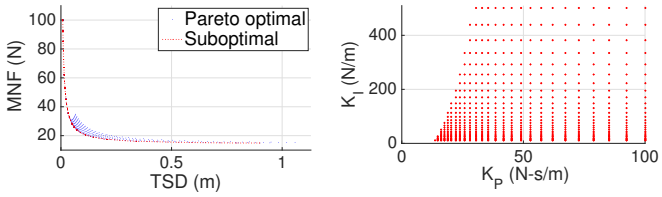

(a) (b)

Fig. 8. MPI control with $v_0 = 1$ m/s. a) shows the resulting tradeoff between MNF and TSD, and highlights the Pareto-optimal fronts, while b) shows the corresponding values of the Pareto-optimal gains. For MPI control, suboptimal MNF/TSD points are significantly less scattered as compared to PI control.

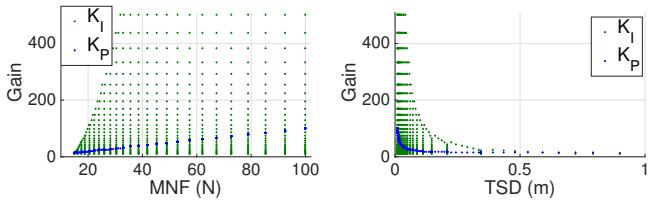

(a) (b)

Fig. 9. MPI control with $v_0 = 1$ m/s. a) shows the Pareto-optimal gains K_P and K_I versus MNF, while b) shows the same gains versus TSD.

5) Dependence of MPI Control on Initial Velocity: To investigate the effect of initial velocity on the closed-loop performance, consider $v_0 \in \{1, 2, 3\}$ m/s, and construct Pareto-optimal fronts for K_P ranging from 10 N-s/m to 100 N-s/m and K_I ranging from 10 N/m to 500 N/m. Figure 10 shows the Pareto-optimal front and corresponding Pareto-optimal gains. For all considered v_0, TSD approaches zero as MNF goes to infinity. Furthermore, MNF and TSD increase as v_0 increases.

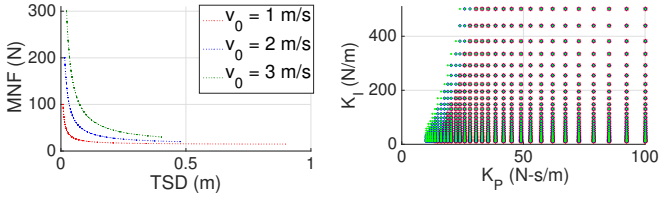

(a) (b)

Fig. 10. MPI control with $v_0 \in \{1, 2, 3\}$ m/s. a) shows the Pareto-optimal front, while b) shows the corresponding Pareto-optimal gains K_I and K_P. Note that the corresponding Pareto-optimal gains are essentially the same for all values of v_0.

IV. Robustness Analysis for MPI Control

A. Robustness to Actuator Dynamics

Actuator mechanism adjusts the position of the end effector fingers to apply the normal force f_n according to the request from the controller. Due to the internal dynamics of the actuator, the applied normal force may differ from the controller request. Let normal force applied by the end effector is given by

$$\dot{f}_\mathrm{n} = -(1/T_\mathrm{act}) f_\mathrm{n} + u. \tag{14}$$

where u is the normal force requested by the controller, and T_{act} is the time constant that defines the bandwidth of the actuator dynamics. For robustness analysis to unmodeled actuator dynamics, consider $T_{\text{act}} \in \{0, 0.05, 0.1\}$ s and, using MPI control, construct Pareto-optimal fronts for K_{P} ranging from 10 N-s/m to 100 N-s/m and K_{I} ranging from 10 N/m to 500 N/m. Figure 11 shows the Pareto-optimal fronts and the corresponding Pareto-optimal gains.

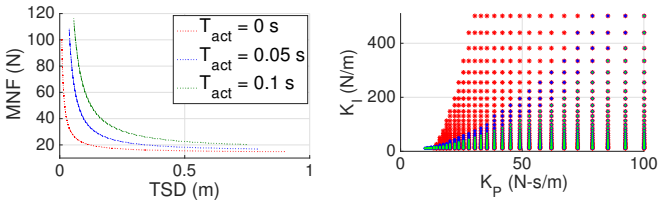

(a) (b)

Fig. 11. MPI control for stabilization and gravity compensation with $v_0 = 1$ m/s and $T_{\text{act}} \in \{0, 0.05, 0.1\}$ s. a) shows the Pareto-optimal fronts, while b) shows the corresponding Pareto-optimal gains K_{I} and K_{P} for each value of T_{act}.

B. Robustness to Constant Disturbances (Uncertain Mass)

As it was mentioned above, robustness to constant disturbances is equivalent to robustness to mass uncertainty. We consider $m \in \{0.8, 1, 1.2\}$ kg, and, using MPI control, we construct Pareto-optimal fronts for K_{P} ranging from 10 N-s/m to 100 N-s/m and K_{I} ranging from 10 N/m to 500 N/m. The Pareto-optimal fronts and the corresponding Pareto-optimal gains are shown in Fig. 12.

C. Robustness to Uncertain Friction

To assess robustness against uncertainties arising from friction parameters uncertainty, we increase and decrease of the nominal friction parameters by 20% and, for each case, applying MPI control, construct Pareto-optimal fronts for K_{P} ranging from 10 N-s/m to 100 N-s/m and K_{I} ranging from 10 N/m to 500 N/m. Note that smaller friction coefficients yield a more slippery surface, and thus a larger slip distance is expected. Figure 13 shows the Pareto-optimal fronts and the corresponding Pareto-optimal gains.

D. Robustness to measurement noise

In numerical study, measurement noise is simulated as a bandlimited Gaussian white noise with zero mean. To investigate robustness of the MPI controller to measurement noise, we consider two levels of noise, namely, level 1 with power spectral density 10^{-5} and level 2 with power spectral density 10^{-4}, and construct Pareto-optimal fronts for K_{P} ranging from 10 N-s/m to 100 N-s/m and K_{I} ranging from 10 N/m to 500 N/m. The Pareto-optimal fronts and the corresponding Pareto-optimal gains are shown in Fig. 14.

V. Discussion

This paper presents a novel force-feedback control for slip suppression for a two-fingered robotic end effector. Under the assumption that slip velocity is measurable, the controller determines the normal force to bring the slip velocity to zero as quickly as possible and with the smallest possible

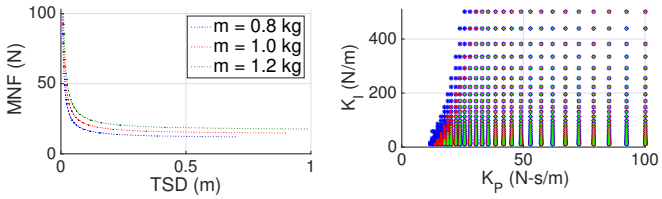

(a) (b)

Fig. 12. MPI control for stabilization and gravity compensation with $v_0 = 1$ m/s and $m \in \{0.8, 1, 1.2\}$ kg. a) shows the Pareto-optimal fronts for K_{P} ranging from 10 N-s/m to 100 N-s/m and for K_{I} ranging from 10 N/m to 500 N/m. b) shows that the Pareto-optimal gains K_{I} and K_{P} are essentially the same for all considered values of m.

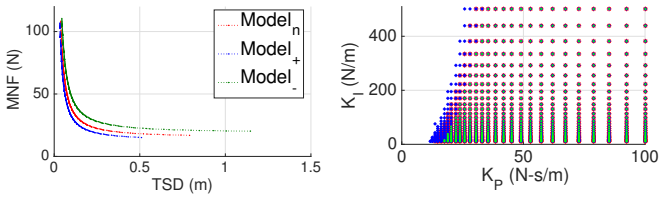

(a) Coulomb friction (b) Coulomb friction

Fig. 13. MPI control for stabilization and gravity compensation with $v_0 = 1$ m/s. a) shows the Pareto-optimal fronts, where Model_{n} stands for the friction model with nominal parameters, while Model_{-} and Model_{+} represent friction models with nominal parameters decreased and increased by 20%, respectively. b) shows that the Pareto-optimal gains K_{I} and K_{P} are essentially the same for the considered values of friction parameters.

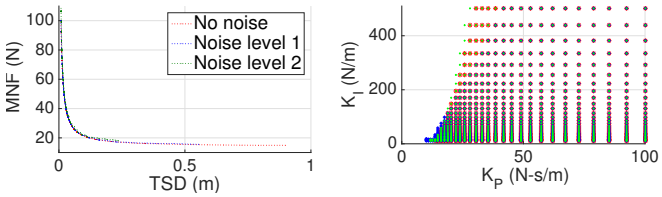

(a) Coulomb friction (b) Coulomb friction

Fig. 14. MPI control for stabilization and gravity compensation with $v_0 = 1$ m/s and measurement noise. a) shows the Pareto-optimal fronts with measurement noise of level 1, 2, and without measurement noise. Note that measurement noise does not significantly effect the Pareto-optimal fronts. b) shows that the Pareto-optimal gains K_{I} and K_{P} are essentially the same for considered noise levels.

slip distance. Since gravity represents a constant disturbance, we focus on the disturbance-rejection problem with a step disturbance, which corresponds to uncertainty in the mass of the body, which, in practice, may be unknown. A convenient approach to disturbance rejection is proportional-integral (PI) control, which is effective despite uncertainty in the external disturbance. Note that, since the friction model is nonlinear and, by assumption, uncertain, classical optimal control strategies are not applicable.

The Pareto-front analysis is based on the tradeoff between two performance metrics, namely, maximum normal force (MNF) and total slip distance (TSD). The goal of the numerical study was to determine the resulting MNF and TSD values for a range of the feedback gains, and obtain the Pareto-optimal front. Analysis of the closed-loop response with PI control showed that, when the control action transitions from predominantly proportional to predominantly integral, the normal force decreases. This phenomenon suggested a novel

modification of linear PI control, namely, the MPI control law, which more efficiently utilizes the normal force without increasing MNF. An immediate benefit of MPI control is that, for a range of proportional and integral gains, the resulting MNF and TSD values are clustered more closely along the Pareto-optimal front. In practical applications, the Pareto-optimal front can be used to determine a feasible set of feedback gains for the MPI control law. Assuming that an estimate of the maximum allowable normal force and body length are available, for a given initial slip velocity and mass, these bounds form a feasible rectangle in the MNF/TSD space. If at least some arc of the Pareto-optimal front lies inside the feasible rectangle, then each PI feedback gain corresponding to each point on the enclosed arc of the Pareto-optimal front is feasible, as shown in Fig. 15. However, if no arc of the Pareto-optimal front lies inside the feasible rectangle then slip suppression is impossible for the given initial velocity, mass, and friction level.

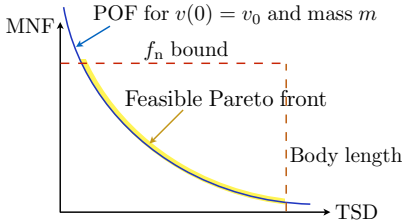

Fig. 15. Pareto-optimal front (POF) for given v_0 and m; the feasible Pareto front is defined by upper bounds on the allowable normal force f_{n} and the body length.

VI. Conclusions

In this work we proposed a novel slip-suppression control law for a two-fingered robotic end effector, where the objective is to minimize the slip distance without using excessive force. As a nonlinear extension of linear proportional-integral (PI) control, the normal force specified by the monotonic PI (MPI) control law is prohibited from decreasing during the transition from predominantly proportional control to predominantly integral control as occurs in the case of linear PI control. Using Pareto-front analysis to compare MPI to PI control, MPI was found to provide performance that was consistently closer to Pareto optimality in terms of the trade-off between maximum normal force (MNF) and total slip distance (TSD). Robustness analysis of MPI control focused on robustness to constant disturbances, uncertain friction, actuator dynamics, and measurement noise. Future research will consider Pareto analysis of MPI control with alternative friction models as well as implementation of MPI control with minimal knowledge of the friction characteristics.

Acknowledgment

This work is supported by a NPRP grant from the Qatar National Research Fund under the grant No. NPRP 7-673-2-251. The statements made herein are solely the responsibility of the authors.

References

[1] H. Yussof, M. Ohka, H. Suzuki, and N. Morisawa, "Tactile sensing-based control algorithm for real-time grasp synthesis in object manipulation tasks of humanoid robot fingers," in *Int. Symp. Robot Human Interactive Comm.*, Aug 2008, pp. 377–382.

[2] L. Roberts, G. Singhal, and R. Kaliki, "Slip detection and grip adjustment using optical tracking in prosthetic hands," in *Int. Conf. IEEE Eng. Medicine Biology Society*, August 2011, pp. 2929–2932.

[3] C. F. Pasluosta, H. Tims, and A. W. . Chiu, "Slippage sensory feedback and nonlinear force control system for a low cost prosthetic hand," *Amer. J. Biomed. Sci.*, vol. 1, no. 4, pp. 295–302, 2009.

[4] E. D. Engeberg and S. G. Meek, "Adaptive object slip prevention for prosthetic hands through proportional-derivative shear force feedback," in *IEEE/RSJ Int. Conf. Intell. Robots Sys.*, Sept 2008, pp. 1940–1945.

[5] B. B. Edin, L. Ascari, L. Beccai, S. Roccella, J.-J. Cabibihan, and M. C. Carrozza, "Bio-inspired sensorization of a biomechatronic robot hand for the grasp-and-lift task," *Brain Rese Bull*, vol. 75, no. 6, pp. 785–795, Apr 2008.

[6] E. D. Engeberg and S. G. Meek, "Adaptive sliding mode control for prosthetic hands to simultaneously prevent slip and minimize deformation of grasped objects," *IEEE/ASME Trans. Mechatronics*, vol. 18, no. 1, pp. 376–384, February 2013.

[7] D. Gunji, Y. Mizoguchi, S. Teshigawara, A. Ming, A. Namiki, M. Ishikawaand, and M. Shimojo, "Grasping force control of multi-fingered robot hand based on slip detection using tactile sensor," in *2008 IEEE International Conference on Robotics and Automation*, May 2008, pp. 2605–2610.

[8] N. Wettels, V. J. Santos, R. S. Johansson, and G. E. Loeb, "Biomimetic tactile sensor array," *Adv. Rob.*, vol. 22, no. 8, pp. 829–849, 2008.

[9] L. Osborn, W. W. Lee, R. Kaliki, and N. Thakor, "Tactile feedback in upper limb prosthetic devices using flexible textile force sensors," in *RAS/EMBS Int. Conf. Biomed. Rob. Biomechatronics*, 2014, pp. 114–119.

[10] G. Cadoret and A. M. Smith, "Friction, not texture, dictates grip forces used during object manipulation," vol. 75, no. 5, pp. 1963–1969, 1996.

[11] M. K. O. Burstedt, J. R. Flanagan, and R. S. Johansson, "Control of grasp stability in humans under different frictional conditions during multidigit manipulation," vol. 82, no. 5, pp. 2393–2405, 1999.

[12] W. W. Lee, J.-J. Cabibihan, and N. V. Thakor, "Bio-mimetic strategies for tactile sensing," in *2013 IEEE SENSORS*, Nov 2013, pp. 1–4.

[13] G. Westling and R. S. Johansson, "Responses in glabrous skin mechanoreceptors during precision grip in humans," *Exp. Brain Research*, vol. 66, no. 1, pp. 128–140, 1987.

[14] S. Andersson, A. Söderberg, and S. Björklund, "Friction models for sliding dry, boundary and mixed lubricated contacts," *Tribology Int.*, vol. 40, no. 4, pp. 580–587, 2007.

[15] M. A. Janaideh and D. S. Bernstein, "Adaptive control of mass-spring systems with unknown hysteretic contact friction," in *Proc. Amer. Contr. Conf.*, July 2016, pp. 667–672.

[16] A. K. Padthe, B. Drincic, J. Oh, D. D. Rizos, S. D. Fassois, and D. S. Bernstein, "Duhem modeling of friction-induced hysteresis," *IEEE Contr. Sys. Mag.*, vol. 28, no. 5, pp. 90–107, 2008.

[17] K. Astrom and C. Canudas de Wit, "Revisiting the lugre friction model," *IEEE Control Systems*, vol. 28, no. 6, pp. 101–114, 2008.

[18] F. Al-Bender, V. Lampaert, and J. Swevers, "Modeling of dry sliding friction dynamics: From heuristic models to physically motivated models and back," *Chaos: An Interdisciplinary J. Nonlinear Science*, vol. 14, no. 2, pp. 446–460, 2004.

[19] B. B. Edin, L. Beccai, L. Ascari, S. Roccella, J.-J. Cabibihan, and M. C. Carrozza, "Bio-inspired approach for the design and characterization of a tactile sensory system for a cybernetic prosthetic hand," in *Proceedings 2006 IEEE International Conference on Robotics and Automation, 2006. ICRA 2006.*, May 2006, pp. 1354–1358.

[20] C. Melchiorri, "Slip detection and control using tactile and force sensors," *IEEE/ASME Trans. Mechatronics*, vol. 5, no. 3, pp. 235–243, Sep 2000.

[21] M. M. Fateh, "Variable structure slip control for grasping objects," in *Int. Conf. Dynam. Sys. Contr.*, 2006.

[22] X. Song, H. Liu, J. Bimbo, K. Althoefer, and L. D. Seneviratne, "A novel dynamic slip prediction and compensation approach based on haptic surface exploration," in *2012 IEEE/RSJ Int. Conf. Intelligent Robots and Systems*, Oct 2012, pp. 4511–4516.

[23] S. P. Bhat and D. S. Bernstein, "Arc-length-based lyapunov tests for convergence and stability with applications to systems having a continuum of equilibria," *Math. Contr. Sig. Sys.*, vol. 22, no. 2, pp. 155–184, 2010.

[24] ——, "Finite-time stability of continuous autonomous systems," *SIAM J. Contr. Opt.*, vol. 38, no. 3, pp. 751–766, 2000.